fluids

MDPI

Article

Numerical Study on Collisions of Solitons of Surface Waves in Finite Water Depth

Bo Liao [1], Guohai Dong [2], Yuxiang Ma [2,*] and Xiaozhou Ma [2]

[1] School of Mathematics and Statistics, Guangxi Normal University, Guilin 541004, China; hylb3020@sina.com
[2] State Key Laboratory of Coastal and Offshore Engineering, Dalian University of Technology, Dalian 116024, China
* Correspondence: yuxma@126.com; Tel.: +86-411-84708526

Abstract: Head-on collisions between two solitary waves in the framework of the nonlinear Schrödinger (NLS) equation were investigated using the Fourier spectral method. When solitary waves undergo collision, the peak value of surface elevation (hereafter referred to as $\zeta_{\max}$) exhibits fluctuations with increasing relative water depths k_0h (where k_0 is the wave number and h is the water depth). $\zeta_{\max}$ is approximately equal to the sum of the peak values of the two solitary waves with smaller wave steepness ε_0 ($\varepsilon_0 = k_0a_0$, a_0 is the free background amplitude parameter), and it exhibits fluctuations for $\varepsilon_0 > 0.10$. Similar results have been observed in the study of head-on collisions for four solitary waves. These results show that the water depth and wave steepness play important roles in the collision of solitary waves, and the effects of the interactions of intense wave groups are important in studies of the mechanisms and manifestations of freak oceanic waves.

Keywords: solitary waves; collision; nonlinear Schrödinger equation; water waves; Fourier spectral method

check for updates

Citation: Liao, B.; Dong, G.; Ma, Y.; Ma, X. Numerical Study on Collisions of Solitons of Surface Waves in Finite Water Depth. *Fluids* **2023**, *8*, 125. https://doi.org/10.3390/fluids8040125

Academic Editors: Yuri V. Lvov and D. Andrew S. Rees

Received: 24 February 2023
Revised: 24 March 2023
Accepted: 30 March 2023
Published: 3 April 2023

Copyright: © 2023 by the authors. Licensee MDPI, Basel, Switzerland. This article is an open access article distributed under the terms and conditions of the Creative Commons Attribution (CC BY) license (https://creativecommons.org/licenses/by/4.0/).

1. Introduction

Some studies have considered the frontal collision of two equal solitary waves both numerically and experimentally. Maxworthy [1] conducted experiments on the frontal collision of two solitary waves and found that the maximum amplitude of these waves can reach twice the initial amplitude. Su and Mirie [2] considered the frontal collision between two solitary waves on the surface of an inviscid uniform fluid and found that the waves generated by the collision maintained their original characteristics with third-order accuracy. Using a set of approximate equations derived by Su and Gardner [3], Mirie and Su [4] presented a numerical calculation of the collisions of two solitary waves and checked the phase shifts and maximum amplitude of the collision with a corresponding perturbation calculation. In addition, Akhmediev and Ankiewicz [5] considered a linear coupler formed by two intersecting solitons. When the soliton amplitudes are equal, the transmission coefficient depends on the collision angle; however, this coefficient does not depend on the relative phase of the solitons. Cook et al. [6] simulated the high-amplitude reflection of solitary waves on a vertical wall based on the boundary element method, and found that solitary waves can be converted into a series of dispersive waves after hitting the wall. Craig et al. [7] proposed a numerical analysis based on the pseudo-spectral method to solve completely nonlinear equations and study the residual generated by the head-on collision of two solitary waves. Chamberel et al. [8] numerically studied head-on collisions of two equal and two unequal steep solitary waves, and found that when the normalized amplitude a_0/h of a solitary wave is greater than 0.60, a thin residual jet will appear. Recently, Slunyaev et al. [9] studied strongly solitary wave groups of collinear surface waves using numerical simulations and laboratory experiments with Euler equations. The maximum displacement of a head-on collision is the sum of the two sets of peak amplitudes. Wave trains with modulational instability [10,11], which transform

into envelope solitons, may lead to huge wave events, and the nonlinear interaction of solitons is a possible physical mechanism of freak wave (the wave height exceeds at least 2.2 times the significant wave height) generation [12]. Interactions of solitary waves were investigated by simulating their collisions in a variety of wave contexts, such as plasma [13], optical fibers [14], and Bose–Einstein condensates [15,16]. Head-on collisions between two solitary waves in plasma have been studied through experiments [17,18] and numerical simulations using the particle-in-cell method [19]. Zhang et al. [19] found that the maximum amplitude during the collision process is less than the sum of the two amplitudes of the envelope solitary waves, and no phase shift was observed after the two envelope solitary waves collided head-on. The head-on collision of two envelope solitary waves was also studied analytically [20].

Some new exact traveling wave solutions and solitary wave solutions for nonlinear partial differential equations have been obtained [21–23]. These new solutions have many applications in other branches of physics and applied science. However, they are rarely used to systematically study the collision of solitary waves: the peak value of surface elevation, $\zeta_{\max}$, is affected by the relative water depth and wave steepness. For a long time, NLS equations have been used to simulate the propagation of waves in finite deep water. Benilov et al. [24] studied the solitary wave solution of NLS with variable coefficients, which controls the weakly nonlinear envelope of surface gravity waves on topography. Grimshaw and Annenkov [25] developed higher-order NLS equations with variable coefficients to describe how a water wave packet will deform and eventually be destroyed as it propagates shoreward from deep to shallow water. Rajan and Henderson [26] considered a variable coefficient dissipative NLS equation, found a solution with uniform amplitude in an appropriate reference frame, and checked its linear stability. Grimshaw [27] deduced a two-dimensional long wave equation with small but limited amplitude in variable depth; the differential equation describing the slow change in the parameters of the solitary wave was derived and solved when the solitary wave evolved from a uniform depth region. Benilov and Howlin [28] studied the evolution of surface gravity wave packets in channels with terrain, where the terrain scale is far smaller than the limit of nonlinear/dispersion scale. Rajan et al. [29] analyzed narrow-banded, periodic one-dimensional surface gravity carrier waves propagating on water of variable depth. Many contemporary researchers have carried out work on soliton collision but have not considered the role of water depth and wave steepness in soliton collision, which is the main purpose of this paper. In this study, the effects of surface tension were neglected; the analysis focused on gravity waves. It is well known that FSM is a powerful tool for solving partial differential equations (PDEs) both theoretically and numerically [30,31]. With the emergence of fast Fourier transform (FFT), Fourier spectral methods can provide a numerical discretization with so-called finite order convergence and high accuracy. In fact, for high-dimensional problems with periodic boundary conditions, the efficiency of the Fourier spectral method is equivalent to that of the finite difference method.

Based on the highly accurate FSM, we solved the NLS equation for gravity waves in finite water depth, as detailed in Section 2. Results of the numerical studies on generation and interactions of the solitary groups are presented in Section 3. The final discussion is reported in Section 4.

2. Numerical Simulation for the NLS Equation

In dimensional variables, the following form is used:

$$i(A_t + c_g A_x) + \alpha A_{xx} + \beta |A|^2 A = 0 \tag{1}$$

where the complex wave envelope $A = A(x, t)$; x is the horizontal coordinate; and t is time. The coefficients in the equation depending on the local water depth have the following definitions [32]:

$$\alpha = -\frac{c_g^2}{2\omega} + \frac{\omega_0 q \cosh^2 q}{k_0^2 \sinh 2q} - \frac{q \sinh q}{k_0 \cosh q} c_g, \tag{2}$$

$$\beta = -\frac{\omega_0 k_0^2 (\cosh 4q + 8 - 2\tanh^2 q)}{16 \sinh^4 q} + \frac{\omega_0}{2\sinh^2 2q} \frac{(2\omega_0 \cosh^2 q + k_0 c_g)^2}{(gh - c_g^2)}, \tag{3}$$

where ω_0 is the carrier wave angular frequency, which follows the following linear dispersion relationship:

$$\omega_0^2 = g k_0 \sigma, \tag{4}$$

where

$$\sigma = \tanh q, \quad q = k_0 h, \quad c = \frac{\omega_0}{k_0} \tag{5}$$

Here, k_0, h, and c denote the wave number, water depth, and wave phase velocity, respectively. c_g denoting the group velocity can be written as follows:

$$c_g = \frac{\omega_0}{2k_0}\left(1 + \frac{2q}{\sinh 2q}\right). \tag{6}$$

The dimensionless variables are presented as follows [33]:

$$A = a_0 A', \quad \varepsilon_0 \omega_0 \gamma_0 (\frac{1}{c_g} x - t) = \xi, \quad \varepsilon_0^2 k_0 x = \eta, \quad \varepsilon_0 \gamma_0 k_0 h = h' \tag{7}$$

where $\varepsilon_0 = k_0 a_0$ is the wave steepness, a_0 is the free background amplitude parameter, and γ_0 is a scale factor that renders the computational domain in ξ to 2π. The evolution of the complex envelope of surface elevation A (ξ, η) can be described using the spatial NLS equation:

$$iA'_\eta + \gamma_0^2 \frac{\overline{\alpha}}{\overline{c}_g^3} A'_{\xi\xi} + \frac{\overline{\beta}}{\overline{c}_g} |A'|^2 A' = 0 \tag{8}$$

where

$$\overline{\alpha} = \alpha \frac{k_0^2}{\omega_0}, \quad \overline{\beta} = \beta \frac{1}{\omega_0 k_0^2}, \quad \overline{c}_g = c_g k_0 / \omega_0 \tag{9}$$

The dimensionless form of the focusing NLS equation is convenient to use:

$$iA'_{\overline{\eta}} + A'_{\overline{\xi}\overline{\xi}} + 2|A'|^2 A' = 0 \tag{10}$$

which results from Equation (8) under the following transformation ($k_0 h > 1.363$):

$$\overline{\eta} = \frac{\overline{\beta}}{2\overline{c}_g} \eta, \quad \overline{\xi} = \frac{\overline{c}_g}{\gamma_0} \sqrt{\frac{\overline{\beta}}{2\overline{\alpha}}} \xi \tag{11}$$

The localized solution of the NLS equation is the envelope soliton, which is presented in the following expression [34]:

$$A'(\overline{\xi}, \overline{\eta}) = \operatorname{sech}(\overline{\xi}) \exp(i\overline{\eta}) \tag{12}$$

Therefore, Equation (8) yields the soliton solution in the following form:

$$A'(\xi, \eta) = \operatorname{sech}(\frac{\overline{c}_g}{\gamma_0} \sqrt{\frac{\overline{\beta}}{2\overline{\alpha}}} \xi) \exp(i \frac{\overline{\beta}}{2\overline{c}_g} \eta) \tag{13}$$

The surface elevation $\zeta\ (x, t)$ to the leading order is presented as follows:

$$\zeta(x,t) \ = \ \mathrm{Re}\{A(x,t)\exp[i(k_0x - \omega_0 t)]\} \tag{14}$$

A highly accurate Fourier spectral method was used to obtain numerical solutions for Equation (8). The spectral method is introduced by approximating the function as a sum of smooth basis functions [30]:

$$A'(\xi) \approx \sum_{j=0}^{N} a_j \Phi_j(\xi) \tag{15}$$

where $\Phi_j(\xi)$ are polynomials or trigonometric functions, and each aj must be determined.

In practice, the basis functions have many feasible options, such as $\Phi_j(\xi) = e^{ik\xi}$ (the Fourier spectral method). The continuous Fourier transform of $A'(\xi)$, which is transformed into Fourier space with regard to ξ and its inverse Fourier transform, is defined as follows:

$$\hat{A}'(k) \ = \ \frac{1}{2\pi}\int_{-\infty}^{+\infty} e^{-ik\xi} A'(\xi) d\xi \tag{16}$$

$$A'(\xi) \ = \ \int_{-\infty}^{+\infty} \hat{A}'(k) e^{ik\xi} dk \tag{17}$$

Similarly to the continuous Fourier transform, we define the discrete Fourier transform: let the solution interval be [0, 2π]; let $A'(\xi)$ be the solution of Equation (8), then transform it into the discrete Fourier space as follows:

$$\hat{A}'(k) \ = \ \frac{1}{N}\sum_{j=0}^{N-1} A(\xi_j) e^{-ik\xi_j}, \quad -\frac{N}{2} \le k \le \frac{N}{2} - 1, \tag{18}$$

Using the inverse Fourier transform, we can obtain the following equations:

$$A'(\xi_j) \ = \ \sum_{k=-N/2}^{N/2-1} \hat{A}'(k) e^{ik\xi_j}, \quad 0 \le j \le N-1 \tag{19}$$

where $\xi_j = 2\pi j/N$, N is the discrete number, noting that N is an even number. The spatial derivatives can be approximated using fast Fourier transform, whereas the time evolution is obtained using the fourth-order Runge–Kutta integrator [31,35]. Using the discrete Fourier transform and its inverse F and F^{-1}, the Fourier transform operator F can obtain a linear operator:

$$F\left\{A'^{(n)}(\xi)\right\} \ = \ (ik)^n F\left\{A'^{(n)}(\xi)\right\}, \tag{20}$$

where $A'^{(n)}(\xi)$ denotes the n-th order derivative of $A'(\xi)$. When $n = 2$,

$$F\{A'^{(2)}(\xi)\} \ = \ (ik)^2 F\{A'^{(2)}(\xi)\} \tag{21}$$

Using the Fourier transform, Equation (8) becomes

$$\hat{A}'_\eta \ = \ -i\gamma_0^2 \frac{\overline{\alpha}}{\overline{c}_g^3}\overline{k}^2 \hat{A}' + i\frac{\overline{\beta}}{\overline{c}_g} F\{|F^{-1}\{\hat{A}'\}|^2 F^{-1}\{\hat{A}'\}\} \tag{22}$$

with

$$\overline{k} \ = \ \frac{2\pi}{L}[-N/2+1, \ldots, -1, 0, 1, \ldots, N/2] \tag{23}$$

Under periodic boundary conditions on the spatial interval [0, L], L is the spatial domain. Then, the fourth-order Runge–Kutta scheme is used to solve the system of complex ordinary differential Equation (22). Letting

$$\hat{\mathbf{A}} = [\hat{A}'(\xi_0, \eta), \hat{A}'(\xi_1, \eta), \cdots \hat{A}'(\xi_{N-1}, \eta)]^T, \tag{24}$$

$$\mathbf{A} = [A'(\xi_0, \eta), A'(\xi_1, \eta), \cdots A'(\xi_{N-1}, \eta)]^T \tag{25}$$

Equation (22) can be written in the following vector form:

$$\hat{\mathbf{A}}_\eta = \mathbf{F}[\hat{\mathbf{A}}] \tag{26}$$

where $\mathbf{F}$ defines the right-hand side of (22). An initial condition is given to the abovementioned problem:

$$A'(\xi, 0) = \mathrm{sech}(\frac{\bar{c}_g}{\gamma_0}\sqrt{\frac{\bar{\beta}}{2\bar{\alpha}}}\xi) \tag{27}$$

The classical fourth-order Runge–Kutta methods for the system (22) is presented as follows:

$$\begin{aligned} \hat{\mathbf{A}}^{m+1} &= \hat{\mathbf{A}}^m + \tfrac{\Delta\eta}{6}(K_1 + 2K_2 + 2K_3 + K_4) \\ K_1 &= \mathbf{F}[\hat{\mathbf{A}}^m], \\ K_2 &= \mathbf{F}[\hat{\mathbf{A}}^m + \tfrac{\Delta\eta}{2}K_1], \\ K_3 &= \mathbf{F}[\hat{\mathbf{A}}^m + \tfrac{\Delta\eta}{2}K_2], \\ K_4 &= \mathbf{F}[\hat{\mathbf{A}}^m + \Delta\eta K_3], \end{aligned} \tag{28}$$

Figure 1 shows the profile of a soliton with k_0 = 4.8, ε_0 = 0.157, γ_0 = 0.1, h = 1, N = 2048, and step size $\Delta\eta$ = 0.0006, $1 \leq m \leq 20{,}000$, where m denotes the mth time step. We carried out sensitivity analyses on grid size and time step; the results are not dependent on the selection of grid size and time step. However, for simplicity, relevant images are not included here. In the transformed domain, the amplitude and shape of the soliton remain invariant during propagation. Firstly, the accuracy of the evolution envelope equation in the isolated subspace was investigated. Slunyaev et al. [36] studied the stability of deep water waves and the existence of strong nonlinear groups through laboratory and numerical simulations. Figure 2 shows a comparison between experimental and numerical simulated surface elevations at five different locations. The small wave steepness obtained in a physical basin may be due to the specificity of the boundary conditions of the wave generator (Equation (14)) or wave dissipation near the wave generator. Under the same initial conditions, compared with numerical simulation, the standing wave group in laboratory experiments ultimately appears to have a smaller steepness. Therefore, the experimental cases shown in Figure 2 (ε_0 = 0.2) and Figure 3 (ε_0 = 0.30) are compared with the numerical simulations of groups ε_0 = 0.157 and ε_0 = 0.25, respectively. Some deviations between the experimental and numerical results are observed at a relatively larger distance. NLS equation may be very useful in describing the general characteristics of initial narrow band water wave sequences that evolve in deep and intermediate-depth water. However, the focusing characteristics of the deep water NLS equation inevitably led to significant spectral broadening, which violates the basic assumptions used in the derivation of the NLS equation [37], and can lead to deviations between numerical simulation and experimental results. The time frequency analysis shown in Figures 4 and 5 clearly demonstrates the stationary waves.

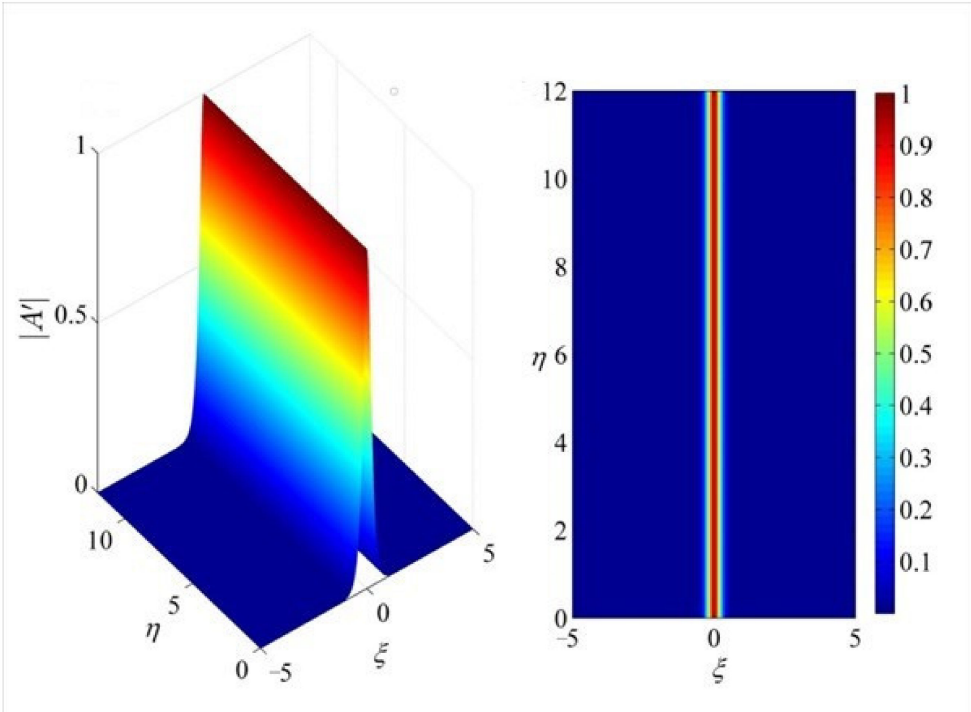

Figure 1. Profile of a soliton with $k_0 = 4.8$, $\varepsilon_0 = 0.157$, $\gamma_0 = 0.1$, $h = 1$, $\Delta\eta = 0.0006$, $N = 2048$.

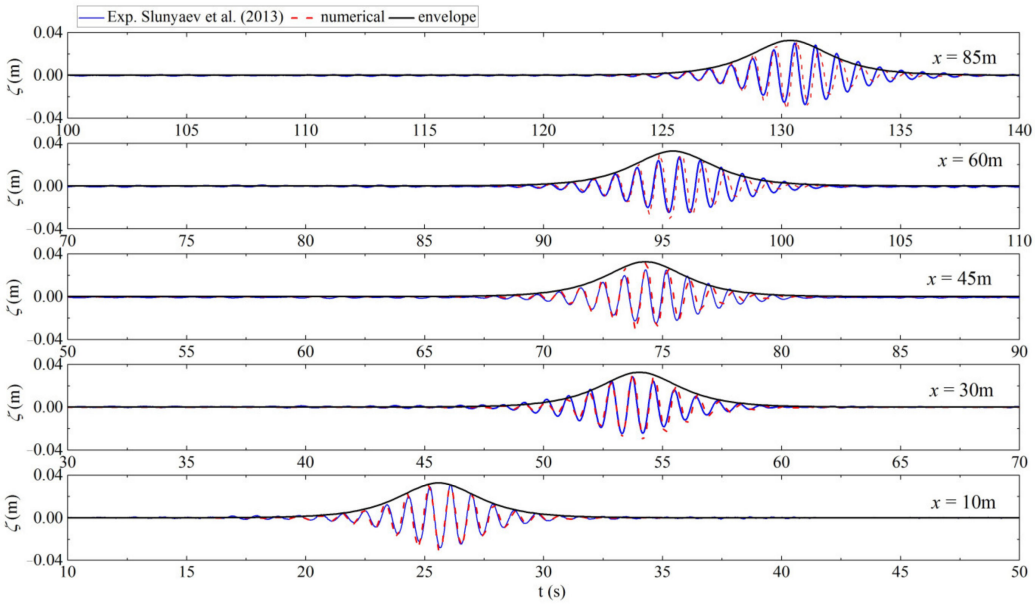

Figure 2. Time series of surface elevation. Blue line: experimental data of Slunyaev et al. [36] ($\varepsilon_0 = 0.2$, $k_0h = 4.8$, $h = 1$, $\omega_0 = 6.86$). Red dashed line: FSM simulation ($\varepsilon_0 = 0.157$, $k_0h = 4.8$, $h = 1$, $\omega_0 = 6.86$). Black dashed dot line: envelope of simulation.

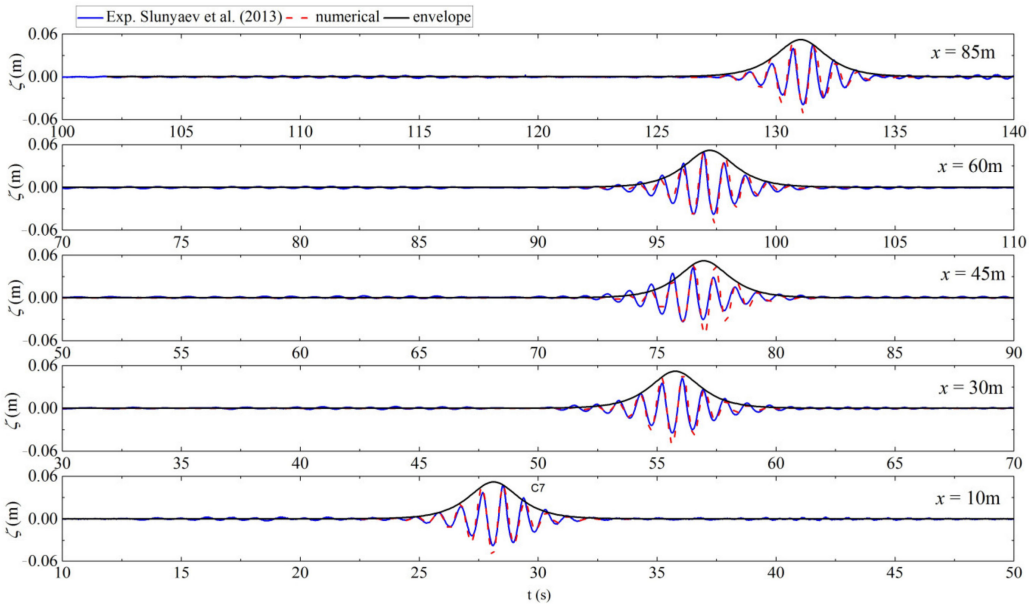

Figure 3. Time series of surface elevation. Blue line: experimental data of Slunyaev et al. [36] (ε_0 = 0.3, k_0h = 4.8, h = 1, ω_0 = 6.86). Red dashed line: FSM simulation (ε_0 = 0.25, k_0h = 4.8, h = 1, ω_0 = 6.86). Black dashed dot line: envelope of simulation.

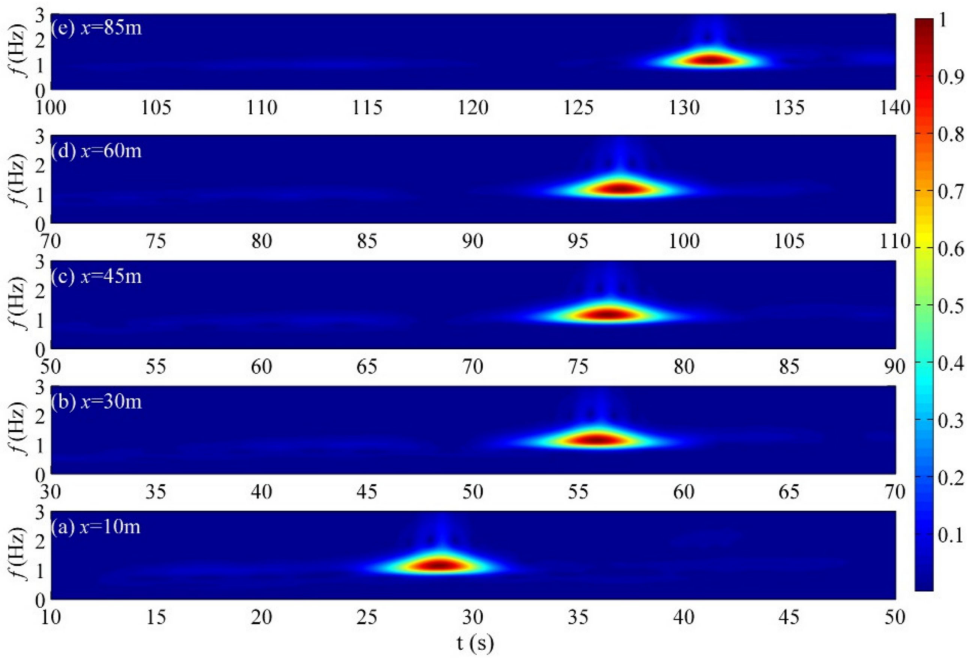

Figure 4. Corresponding wavelet spectrum of measurements depicted in Figure 3.

In this study, the Morlet wavelet was selected as the mother wavelet. The wavelet spectrum was non-dimensionalized by the maximum wavelet energy at each location. Most of the wave energy was distributed near the center frequency of the carrier wave, and the instantaneous frequency of the intermediate wave packet in the wave train was a triangular signal. However, the measured wave heights covered higher-frequency components, and the energy of higher harmonics became significant. Therefore, the numerical simulation was consistent with the experimental measurement results. In addition, the NLS equation can be used to describe the general characteristics of initially narrow band water wave trains that evolve in deep and medium-deep water [37].

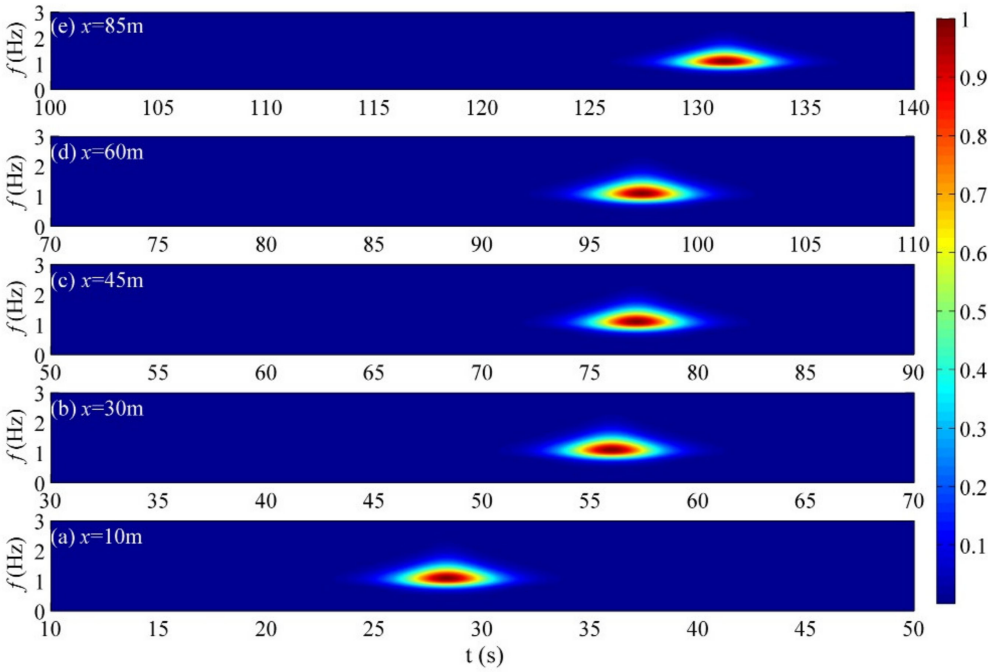

Figure 5. Corresponding wavelet spectrum of FSM simulation in Figure 3.

3. Interaction of Solitons

Wave collision is a common phenomenon in water waves. The collision between two solitary waves manifests in two forms: overtaking collisions (solitary waves propagating in the same direction), and head-on collisions (solitary waves propagating in opposite directions). We selected the following initial conditions to study the interactions between two solitons [5]:

$$\begin{aligned} A'(\xi,0) &= -ib\mathrm{sech}[b\tfrac{\bar{c}_g}{\gamma_0}\sqrt{\tfrac{\bar{\beta}}{2\bar{\alpha}}}(\xi+\xi_1)]\exp(ia_1\tfrac{\bar{c}_g}{\gamma_0}\sqrt{\tfrac{\bar{\beta}}{2\bar{\alpha}}}\xi - i\varphi_1) \\ &\quad -ib\mathrm{sech}[b\tfrac{\bar{c}_g}{\gamma_0}\sqrt{\tfrac{\bar{\beta}}{2\bar{\alpha}}}(\xi+\xi_2)]\exp(ia_2\tfrac{\bar{c}_g}{\gamma_0}\sqrt{\tfrac{\bar{\beta}}{2\bar{\alpha}}}\xi - i\varphi_2) \end{aligned} \tag{29}$$

where b is the amplitude of each solitary wave, and a_1 and a_2 are the "velocities". The values of φ_1 and φ_2 are the initial phases of the wave; when φ_1-φ_2 is 0 or π, the solitary waves are initially in phase. ξ_1 and ξ_2 are the locations of solitons. We only considered the collision of the solitons with equal amplitude and equal velocity but with different directions of movement, and a wave steepness $\varepsilon_0 = k_0 A_0$ ($A_0 = 0.01b$). A head-on collision between two solitary waves is depicted in Figures 6–11. We observed that the amplitudes of the solitary waves were not altered after the interaction, and the solitary waves passed through each other without losing their identity but with a slight phase shift. During collision, the peak value of the amplitude was initially equal to the sum of the peak values of the two solitons. As shown in Figure 7, the water depth, h, increased, whereas the other parameters were kept fixed, and the widths of the two solitary waves became smaller than those shown in Figure 6. Therefore, the shallow-water region contains more waves than the deep water region, and no phase shift in solitary waves is observed in deep water (Figure 7b). Thus, the propagation velocity of the solitary waves is constant. Figures 8 and 9 show the surface elevation of the corresponding head-on collision between the two solitary waves shown in Figures 6 and 7. With the increase in water depth, the distance that the solitons must travel before collision will decrease significantly (i.e., the evolution of the modulational instability is accelerated).

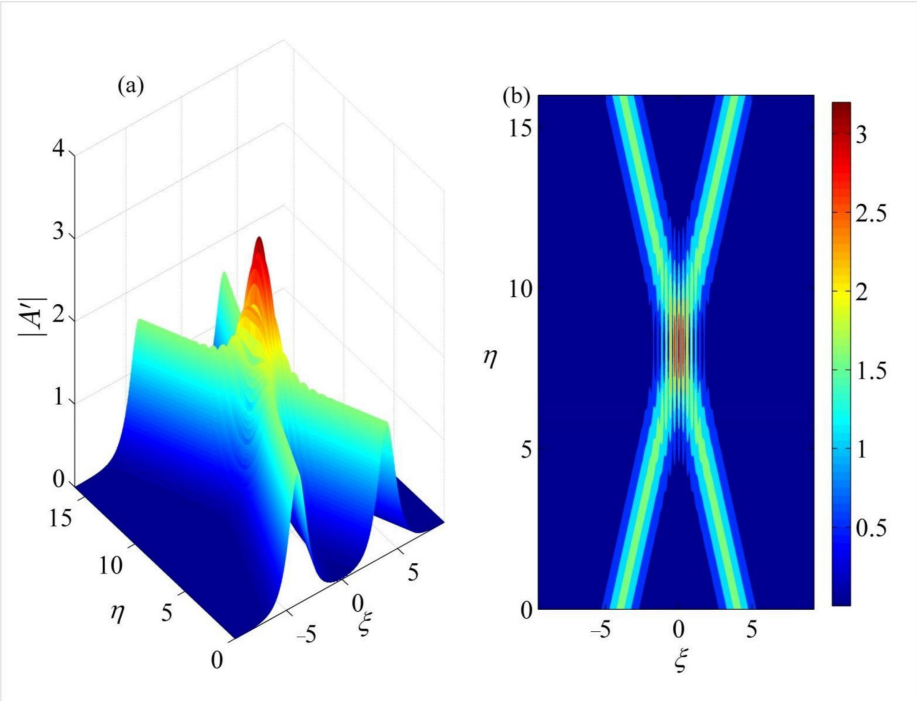

Figure 6. Head-on collision between the two solitary waves $\varepsilon_0 = 0.08$, $k_0 = 5$, $h = 0.28$, $a_1 = -a_2 = 12$, $b = 1.6$, $\xi_1 = -4$, $\xi_2 = 4$, $\varphi_1 = \varphi_2 = 0$ (**a**) (ξ, η)-plot and (**b**) contour plot of the wave amplitudes.

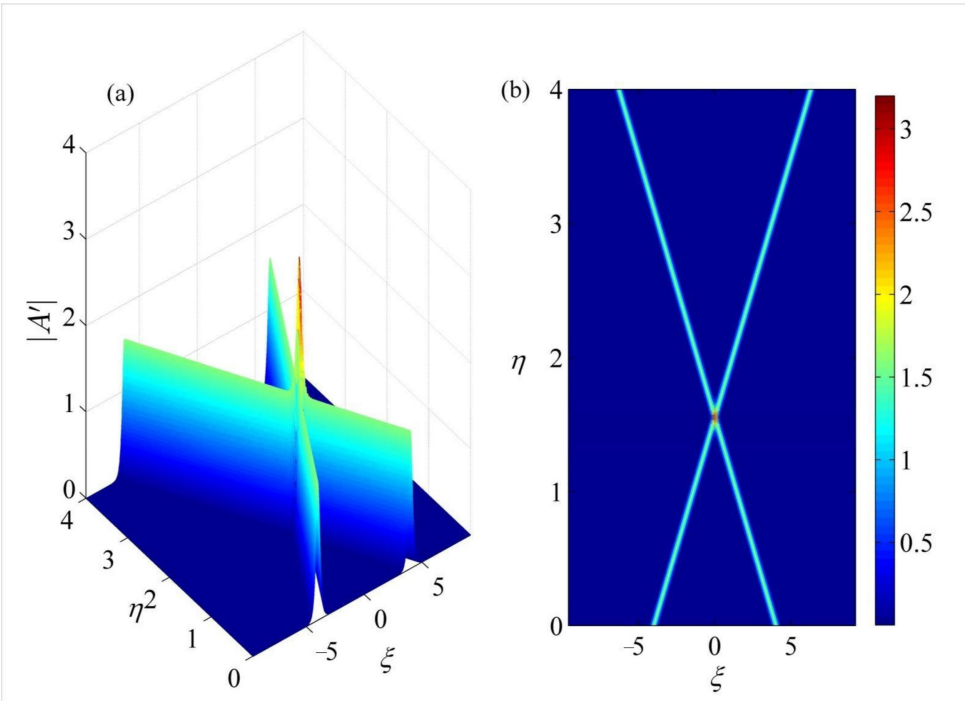

Figure 7. Head-on collision between the two solitons $\varepsilon_0 = 0.08$, $k_0 = 5$, $h = 2$, $a_1 = -a_2 = 12$, $b = 1.6$, $\xi_1 = -4$, $\xi_2 = 4$, $\varphi_1 = \varphi_2 = 0$ (**a**) (ξ, η)-plot and (**b**) contour plot of the wave amplitudes.

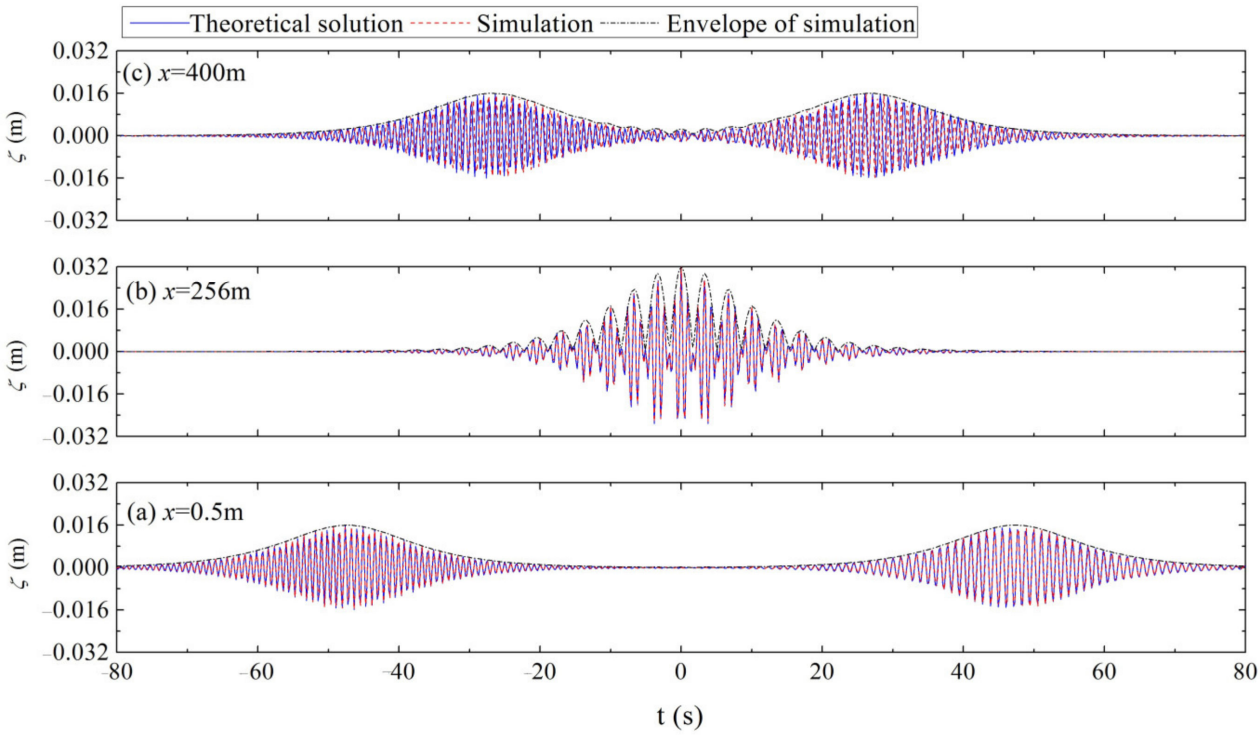

Figure 8. Corresponding time series of the surface elevation of a head-on collision between the two solitons at the different locations shown in Figure 6.

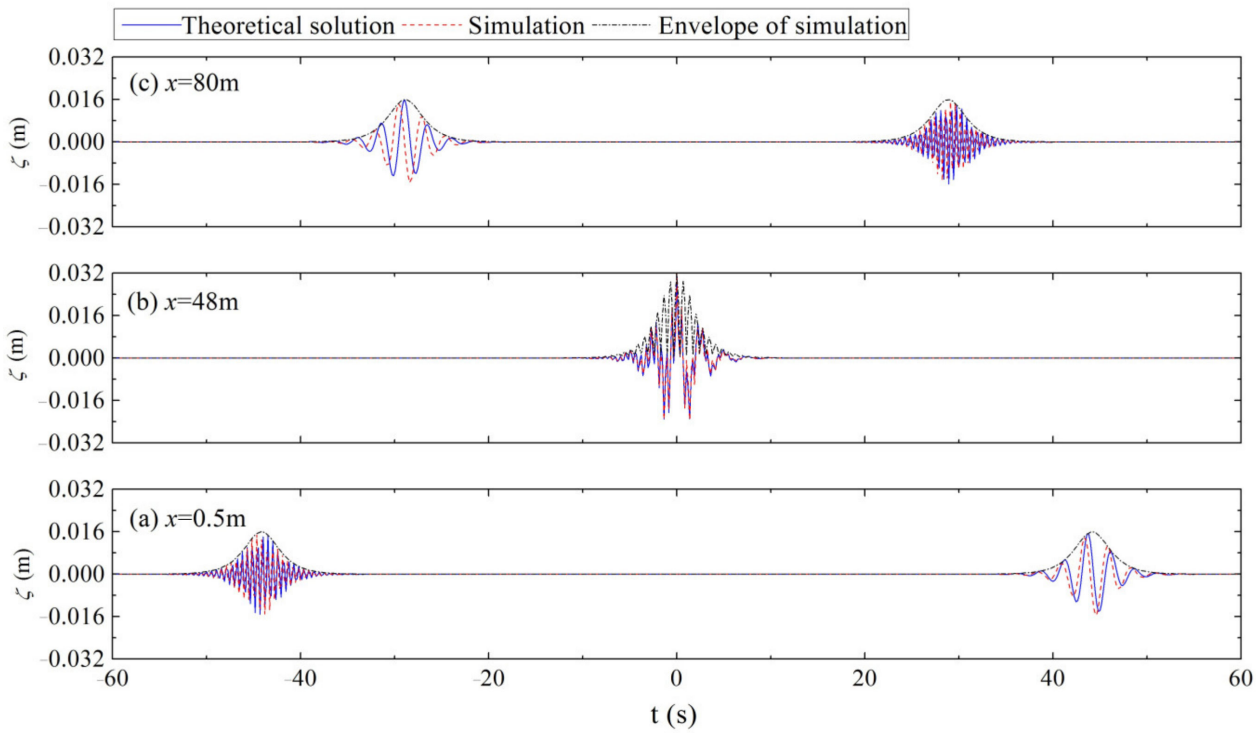

Figure 9. Corresponding time series of the surface elevation of a head-on collision between the two solitons at different locations shown in Figure 7.

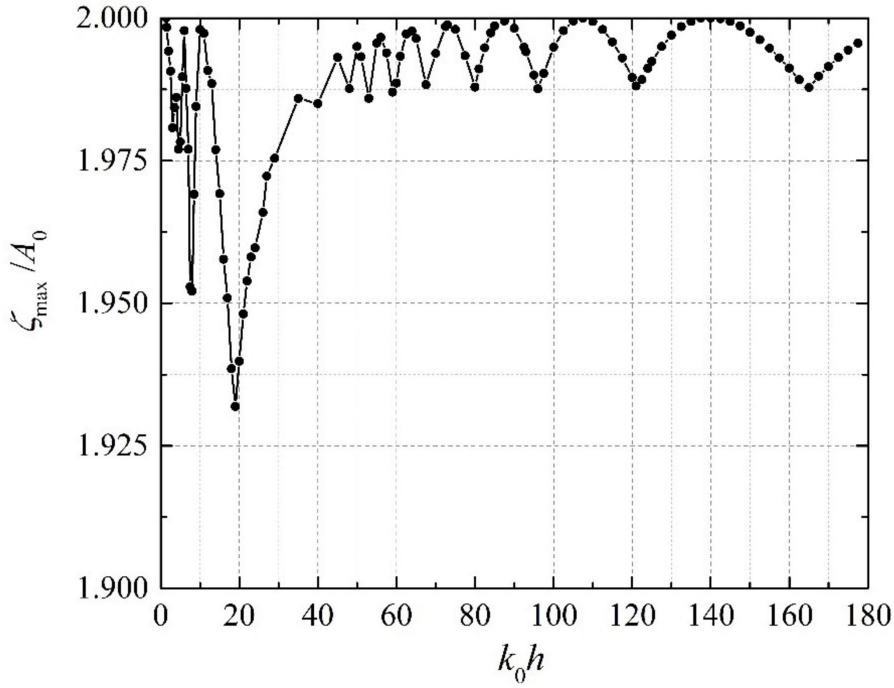

Figure 10. Peak value of the surface elevation versus the relative water depth k_0h with $\varepsilon_0 = 0.08$, $k_0 = 5$, $a_1 = -a_2 = 12$, $b = 1.6$, $\xi_1 = -4$, $\xi_2 = 4$, $\varphi_1 = \varphi_2 = 0$.

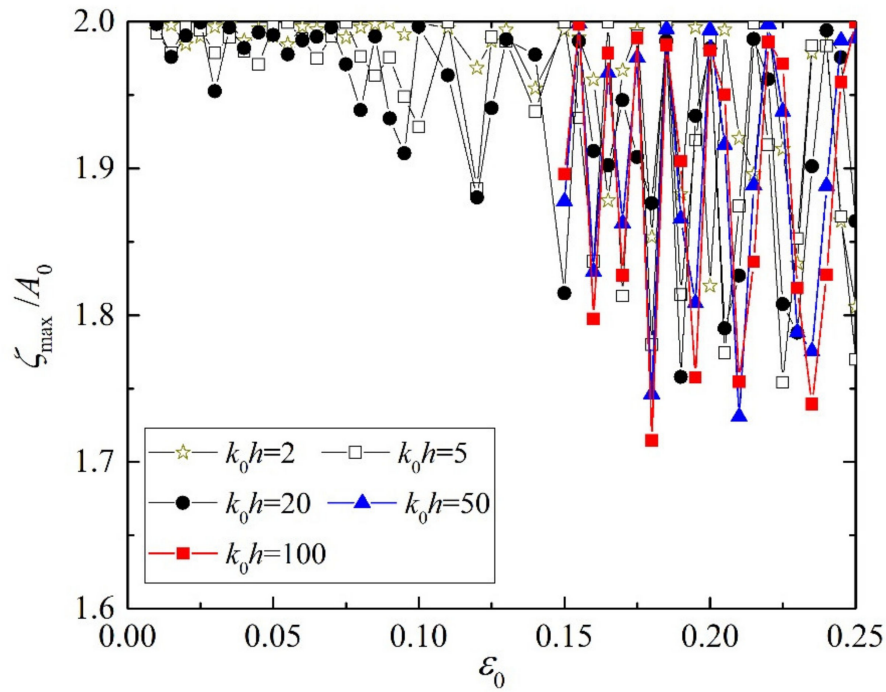

Figure 11. Peak value of the surface elevation versus the wave steepness ε_0 with $b = 1$, $a_1 = -a_2 = 12$, $\xi_1 = -4$, $\xi_2 = 4$, $\varphi_1 = \varphi_2 = 0$.

The effect of water depth, k_0h, on the surface elevation of a corresponding head-on collision between the solitary waves is presented in Figure 10. During the collision, the value of ε_0 is initially equal to the sum of the peak values of the solitary waves, and the wave profile is based on the principle of linear superposition. However, with the increase in water depth, k_0h, ζ_{max} is less than the sum of the peak values of the two solitary waves, which is consistent with the results reported by Slunyaev et al. [9] (the effect of finite depth

reduces the amplitude of the eventual solitary group). $\zeta_{\max}$ exhibits fluctuations with increasing water depths. Figure 11 presents the peak value of surface elevation versus wave steepness, ε_0. In the case of smaller steepness, $\zeta_{\max}$ is approximately equal to the sum of the peak values of the two solitary waves, and it exhibits significant fluctuations for $\varepsilon_0 > 0.10$. These results indicate that the water depth and wave steepness play important roles in the interaction of solitons. We also investigated the interaction of four solitary waves, and the initial condition is given as follows:

$$\begin{aligned} A'(\xi,0) \;=\; & -ib\mathrm{sech}[b\tfrac{\bar{c}_g}{\gamma_0}\sqrt{\tfrac{\bar{\beta}}{2\bar{\alpha}}}(\xi+\xi_1)]\exp(ia_1\tfrac{\bar{c}_g}{\gamma_0}\sqrt{\tfrac{\bar{\beta}}{2\bar{\alpha}}}\xi - i\varphi_1) \\ & -ib\mathrm{sech}[b\tfrac{\bar{c}_g}{\gamma_0}\sqrt{\tfrac{\bar{\beta}}{2\bar{\alpha}}}(\xi+\xi_2)]\exp(ia_2\tfrac{\bar{c}_g}{\gamma_0}\sqrt{\tfrac{\bar{\beta}}{2\bar{\alpha}}}\xi - i\varphi_2) \\ & -ib\mathrm{sech}[b\tfrac{\bar{c}_g}{\gamma_0}\sqrt{\tfrac{\bar{\beta}}{2\bar{\alpha}}}(\xi+\xi_3)]\exp(ia_3\tfrac{\bar{c}_g}{\gamma_0}\sqrt{\tfrac{\bar{\beta}}{2\bar{\alpha}}}\xi - i\varphi_3) \\ & -ib\mathrm{sech}[b\tfrac{\bar{c}_g}{\gamma_0}\sqrt{\tfrac{\bar{\beta}}{2\bar{\alpha}}}(\xi+\xi_4)]\exp(ia_4\tfrac{\bar{c}_g}{\gamma_0}\sqrt{\tfrac{\bar{\beta}}{2\bar{\alpha}}}\xi - i\varphi_4) \end{aligned} \tag{30}$$

As shown in Figure 12, head-on collisions occurred between the four solitary waves ($\varepsilon_0 = 0.08$, $k_0 = 5$, $h = 0.28$, $a_1 = a_2 = 21$, $a_3 = a_4 = 7$, $b = 1.6$, $\xi_1 = \xi_2 = 6$, $\xi_3 = \xi_4 = 2$, $\varphi_1 = \varphi_2 = \varphi_3 = \varphi_4 = 0$), where the four solitary waves retained invariant shapes, except for the phase shifts before and after the collision. During collision, the peak value of surface elevation, $\zeta_{\max}$, was initially equal to the sum of the peak values of the four solitary waves. In addition, the amplification factor was equal to six, which indicated a freak wave. Therefore, the four solitary waves interacted for a short time, and the superposition principle did not hold at the point of interaction in deep water. Figure 13 shows the effect of water depth, k_0h, on the surface elevation of the corresponding head-on collision among the four solitary waves. During collision, the peak value of surface elevation, $\zeta_{\max}$, was initially equal to the sum of the peak values of the solitary waves; however, $\zeta_{\max}$ exhibited significant fluctuations with increasing water depths.

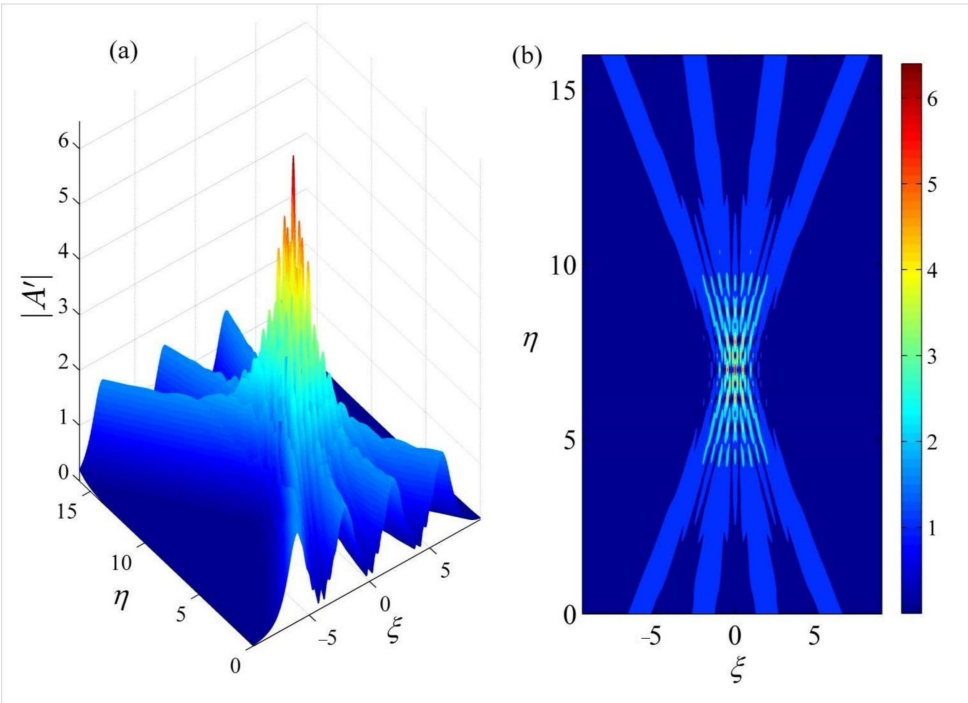

Figure 12. Head-on collision among the four solitary waves $\varepsilon_0 = 0.08$, $k_0 = 5$, $h = 0.28$, $a_1 = -a_2 = 21$, $a_3 = -a_4 = 7$, $b = 1.6$, $\xi_1 = -\xi_2 = 6$, $\xi_3 = -\xi_4 = 2$, $\varphi_1 = \varphi_2 = \varphi_3 = \varphi_4 = 0$ (**a**) (ξ, η)-plot and (**b**) contour plot of the wave amplitudes.

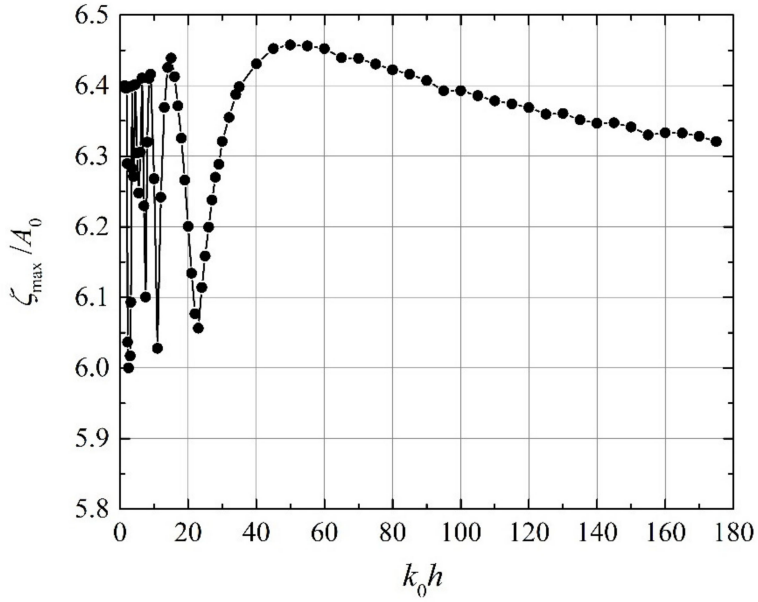

Figure 13. Peak value of the surface elevation versus the relative water depth, k_0h, with $\varepsilon_0 = 0.08$, $k_0 = 5$, $a_1 = -a_2 = 21$, $a_3 = -a_4 = 7$, $b = 1.6$, $\xi_1 = -\xi_2 = 6$, $\xi_3 = -\xi_4 = 2$, $\varphi_1 = \varphi_2 = \varphi_3 = \varphi_4 = 0$.

4. Discussion

In this study, we modelled the solitary wave interactions by solving the NLS equation numerically. First, we solved the NLS equation to determine the spatial evolution of a solitary wave in finite water depth; the results showed good agreement between the numerical simulations and experimental measurements. However, the measured wave elevation covered evidently higher frequency components, and the energy of the higher harmonics became significant. Then, we considered collisions of the solitons with equal amplitudes and equal velocities, but with different directions of movement. During the collision, the solitary waves passed through each other and completely preserve their shapes and velocities, but a slight phase shift was observed. In contrast, no phase shift of the solitary waves was found in deep water. In addition, the peak value of surface elevation, ζ_{max}, exhibited significant fluctuations with increasing water depths, k_0h. In the case of relatively small steepness, ε_0, ζ_{max} was approximately equal to the sum of the peak values of the two interacting solitary waves, and it exhibited significant fluctuations for $\varepsilon_0 > 0.10$ for the head-on collision. However, the mechanism of generation of this phenomenon remains an open problem. Similar results have been observed in studies of head-on collisions of four solitary waves. These results indicate that the water depth and wave steepness play important roles in soliton interactions, and the effects of the interactions of intense wave groups are important to study the mechanisms and manifestations of freak oceanic waves. These new results have many applications in the field of physics and other branches of applied science; such results show great potential for applications in the instability study of plasma and optical fibers. Meanwhile, FSM simulations provide a realistic description of the dynamics of nonlinear waves.

Author Contributions: Formal analysis, B.L.; Funding acquisition, B.L.; Methodology, B.L. and Y.M.; Software, B.L.; Supervision, G.D., Y.M. and X.M.; Writing—original draft, B.L.; Writing—review editing, B.L. and Y.M. All authors have read and agreed to the published version of the manuscript.

Funding: This study was funded by the National Natural Science Foundation of China (Grant No. 51969005) and Guangxi Science and Technology Department Specific Research Project of Guangxi for Research Bases and Talents (Guike AD20159016).

Data Availability Statement: The data that support the findings of this study are available from the corresponding author upon reasonable request.

Acknowledgments: The author thanks Alexey Slunyaev and Marco Klein for the experimental data.

Conflicts of Interest: The authors declare no conflict of interest.

References

1. Maxworthy, T. Experiments on collisions between solitary waves. *J. Fluid Mech.* **1976**, *76*, 177–186. [CrossRef]
2. Su, C.H.; Mirie, R.M. On head-on collisions between two solitary waves. *J. Fluid Mech.* **1980**, *98*, 509–525. [CrossRef]
3. Su, C.H.; Gardner, C.S. Korteweg-de Vries Equation and Generalizations. III. Derivation of the Korteweg-de Vries equation and Burgers equation. *J. Math. Phys.* **1969**, *10*, 536–539. [CrossRef]
4. Mirie, R.M.; Su, C.H. Collisions between two solitary waves. Part 2. A numerical study. *J. Fluid Mech.* **1982**, *115*, 476–492. [CrossRef]
5. Akhmediev, N.; Ankiewicz, A. Spatial soliton X-junctions and couplers. *Opt. Commun.* **1993**, *100*, 186–192. [CrossRef]
6. Cooker, M.J.; Weidman, P.D.; Bale, D.S. Reflection of a high-amplitude solitary wave at a vertical wall. *J. Fluid Mech.* **1997**, *342*, 141–158. [CrossRef]
7. Craig, W.; Guyenne, P.; Hammack, J.; Henderson, D.; Sulem, C. Solitary water wave interactions. *Phys. Fluids* **2006**, *18*, 057106. [CrossRef]
8. Chambarel, J.; Kharif, C.; Touboul, J. Head-on collision of two solitary waves and residual falling jet formation. *Nonlinear Proc. Geoph.* **2009**, *16*, 111–122. [CrossRef]
9. Slunyaev, A.; Klein, M.; Clauss, G. Laboratory and numerical study of intense envelope solitons of water waves: Generation, reflection from a wall, and collisions. *Phys. Fluids* **2017**, *29*, 047103. [CrossRef]
10. Benjamin, T.B.; Feir, J.E. The disintegration of wave trains on deep water Part 1. Theory. *J. Fluid Mech.* **1967**, *27*, 417–430. [CrossRef]
11. Segur, H.; Henderson, D.; Carter, J.; Hammack, J.; Li, C.M.; Pheiff, D.; Socha, K. Stabilizing the Benjamin-Feir in stability. *J. Fluid Mech.* **2005**, *539*, 229–271. [CrossRef]
12. Kharif, C.; Pelinovsky, E. Physical mechanisms of the rogue wave phenomenon. *Eur. J. Mech. B Fluids* **2003**, *22*, 603–634. [CrossRef]
13. Zabusky, N.J.; Kruskal, M.D. Interaction of 'solitons' in a collisionless plasma and the recurrence of initial states. *Phys. Rev. Lett.* **1965**, *15*, 240–243. [CrossRef]
14. Gordon, J.P. Interaction forces among solitons in optical fibers. *Opt. Lett.* **1983**, *8*, 596–598. [CrossRef]
15. Komineas, S.; Brand, J. Collisions of solitons and vortex rings in cylindrical Bose–Einstein condensates. *Phys. Rev. Lett.* **2005**, *95*, 110401. [CrossRef]
16. Nguyen, J.H.V.; Dyke, P.; Luo, D.; Malomed, B.A.; Hulet, R.G. Collisions of matter-wave solitons. *Nat. Phys.* **2014**, *10*, 918–922. [CrossRef]
17. Harvey, P.; Durniak, C.; Samsonov, D.; Morfill, G. Soliton interaction in a complex plasma. *Phys. Rev. E* **2010**, *81*, 057401. [CrossRef]
18. Sharma, S.K.; Boruah, A.; Bailung, H. Head-on collision of dust-acoustic solitons in a strongly coupled dusty plasma. *Phys. Rev. E* **2014**, *89*, 013110. [CrossRef]
19. Zhang, H.; Qi, X.; Duan, W.S.; Yang, L. Envelope solitary waves exist and collide head-on without phase shift in a dusty plasma. *Sci. Rep.* **2015**, *5*, 14239. [CrossRef]
20. El-Labany, S.K.; El-Taibany, W.F.; El-Shamy, E.F.; El-Depsy, A.; Zedan, N.A. Head-on-collision of modulated dust acoustic waves in strongly coupled dusty plasma. *Phys. Plasmas* **2012**, *19*, 103708. [CrossRef]
21. Lu, D.C.; Seadawy, A.R.; Iqbal, M. Mathematical methods via construction of traveling and solitary wave solutions of three coupled system of nonlinear partial differential equations and their applications. *Results Phys.* **2018**, *11*, 1161–1171. [CrossRef]
22. Seadawy, A.R.; Ali, K.K.; Nuruddeen, R.I. A variety of soliton solutions for the fractional Wazwaz–Benjamin–Bona–Mahony equations. *Results Phys.* **2019**, *11*, 2234–2241. [CrossRef]
23. Seadawy, A.R.; Lu, D.C.; Iqbal, M. Application of mathematical methods on the system of dynamical equations for the ion sound and Langmuir waves. *Pramana J. Phys.* **2019**, *93*, 10. [CrossRef]
24. Benilov, E.S.; Flanagan, J.D.; Howlin, C.P. Evolution of packets of surface gravity waves over smooth topography. *J. Fluid Mech.* **2005**, *533*, 171–181. [CrossRef]
25. Grimshaw, R.H.J.; Annenkov, S.Y. Water Wave Packets Over Variable Depth. *Stud. Appl. Math.* **2011**, *126*, 409–427. [CrossRef]
26. Rajan, G.K.; Henderson, D.M. The Linear Stability of a Wavetrain Propagating on Water of Variable Depth. *SIAM J. Appl. Math.* **2016**, *76*, 2030–2041. [CrossRef]
27. Grimshaw, R. The solitary wave in water of variable depth. *J. Fluid Mech.* **1970**, *42*, 639–653. [CrossRef]
28. Benilov, E.S.; Howlin, C.P. Evolution of packets of surface gravity waves over strong smooth topography. *Stud. Appl. Math.* **2006**, *116*, 289–301. [CrossRef]
29. Rajan, G.K.; Bayram, S.; Henderson, D.M. Periodic envelopes of waves over non-uniform depth. *Phys. Fluids* **2016**, *28*, 289042106. [CrossRef]
30. Shen, J.; Tang, T. *Spectral and High-Order Methods with Applications*; Science Press: Beijing, China, 2006; pp. 4–20.
31. Trefethen, L. *Spectral Methods in MATLAB*; SIAM: Philadelphia, PA, USA, 2000; pp. 101–112.
32. Mei, C.C.; Stiassnie, M.; Yue, D.K.P. Narrow-Banded Nonlinear Waves in Water of Intermediate or Great Depth. In *Theory and Applications of Ocean Surface Waves*; Liu, P.L.-F., Ed.; World Scientific: Singapore, 2005; pp. 745–756.

33. Lo, E.; Mei, C.C. A numerical study of water-wave modulation based on higher-order nonlinear Schrödinger equation. *J. Fluid Mech.* **1985**, *150*, 395–416. [CrossRef]
34. Zakharov, V.E.; Shabat, A.B. Exact theory of two-dimensional self-focusing and one-dimensional self-modulation of waves in nonlinear media. *J. Exp. Theor. Phys.* **1972**, *34*, 62–69.
35. Calini, A.; Schober, C.M.; Strawn, M. Linear instability of the Peregrine breather: Numerical and analytical investigations. *Appl. Numer. Math.* **2018**, *141*, 36–43. [CrossRef]
36. Slunyaev, A.; Clauss, G.F.; Klein, M.; Onorato, M. Simulations and experiments of short intense envelope solitons of surface water waves. *Phys. Fluids* **2013**, *26*, 067105. [CrossRef]
37. Shemer, L. Advantages and limitations of the nonlinear Schrödinger equation in describing the evolution of nonlinear water-wave groups. *Proc. Est. Acad. Sci.* **2015**, *64*, 356–360. [CrossRef]

Disclaimer/Publisher's Note: The statements, opinions and data contained in all publications are solely those of the individual author(s) and contributor(s) and not of MDPI and/or the editor(s). MDPI and/or the editor(s) disclaim responsibility for any injury to people or property resulting from any ideas, methods, instructions or products referred to in the content.